Gauge theory couplings on anisotropic lattices

Marcela Carena,[1,2,3,4,*] Erik J. Gustafson,[1,†] Henry Lamm,[1,‡] Ying-Ying Li,[1,§] and Wanqiang Liu[4,‖]

[1]*Fermi National Accelerator Laboratory, Batavia, Illinois 60510, USA*
[2]*Enrico Fermi Institute, University of Chicago, Chicago, Illinois 60637, USA*
[3]*Kavli Institute for Cosmological Physics, University of Chicago, Chicago, Illinois 60637, USA*
[4]*Department of Physics, University of Chicago, Chicago, Illinois 60637, USA*

(Received 7 September 2022; accepted 29 November 2022; published 21 December 2022)

The advantage of simulating lattice field theory with quantum computers is hamstrung by the limited resources that induce large errors from finite volume and sizable lattice spacings. Previous work has shown how classical simulations near the Hamiltonian limit can be used for setting the lattice spacings in real time through analytical continuation, thereby reducing errors in quantum simulations. In this work, we derive perturbative relations between bare and renormalized quantities in Euclidean spacetime at any anisotropy factor—the ratio of spatial to temporal lattice spacings—and in any spatial dimension for $U(N)$ and $SU(N)$. This reduces the required classical preprocessing for quantum simulations. We find less than 10% discrepancy between our perturbative results and those from existing nonperturbative determinations of the anisotropy for $SU(2)$ and $U(1)$ gauge theories. For the discrete groups $\mathbb{Z}_{10}$, $\mathbb{Z}_{100}$ and $\mathbb{BI}$, we perform lattice Monte Carlo simulations to extract anisotropy factors and observe similar agreement with our perturbative results.

DOI: 10.1103/PhysRevD.106.114504

I. INTRODUCTION

Quantum computers can make predictions of nonperturbative quantum field theories beyond the reach of classical resources [1–4]. However, quantum simulations are constrained by limited and noisy resources, and will continue to be so for the foreseeable future. Current estimates suggest ∼10 logical qubits per gluon link should suffice to digitize $SU(3)$ [4–11], with similar requirements for $U(1)$ and $SU(2)$ [4–8,11–31]. The total number of qubits required depends on the phenomena studied; $\mathcal{O}((L/a)^3)$ links are usually required for a $3+1d$ lattice gauge theories, exacerbating the qubit requirement. Quantum error corrections can further introduce an overhead of $\mathcal{O}(10^{1-5})$ [32–34] physical qubits per logical qubit depending on platform. For the gate costs to implement the time evolution of the theory under a lattice Hamiltonian, $\mathcal{O}(10^{49})$ T gates are required to compute the shear viscosity with $\mathcal{O}(10^5)$ logical qubits [9]. This upper bound can be reduced, e.g. by controlling only errors on low-lying states [35,36]. Even with these reductions, quantum resources are far beyond near-term devices. Further, this estimate neglects state preparation, which often dominates the total gate costs [37].

Resources can in principle be reduced by using more clever quantum subroutines and performing better classical processing. Gate reductions may be possible via other approximations of $\mathcal{U}(t)$ [38–43]. Lattice-field-theory specific error correction [44,45] or mitigation [46–57] could help further. Recently, quantum circuits for Hamiltonians with reduced lattice artifacts [58,59] were constructed [60]. A full accounting of resources should also consider any reductions through classical computations. Lattice calculations have a number of steps that can potentially be offloaded to classical resources. The first suggested was to use Euclidean lattice ensembles to perform stochastic state preparation yielding shallower individual circuits [61–64]. Euclidean lattice simulations on classical computers help to quantify the scheme-dependent systematic errors [6,10,19,65–67]. Further, classical simulations can be used to set the scales, which via analytical continuation [68,69] give the lattice spacings of the quantum simulation with few or no quantum resources [70,71].

Although in [70] the connection between lattice Hamiltonian at finite real-time temporal lattice spacing a_t and Euclidean temporal lattice spacing a_τ was made,

*carena@fnal.gov
†egustafs@fnal.gov
‡hlamm@fnal.gov
§Corresponding author.
yingyingli1013@outlook.com
‖wanqiangl@uchicago.edu

the final step of connecting the Hamiltonian to the bare parameters used in Euclidean action was missing. The brute-force approach would compute multiple anisotropies $\xi = a/a_\tau$ for a fixed spatial lattice spacing a and then extrapolate to the desired ξ used in the quantum simulation, analogous to studies of the relation between Euclidean and Hamiltonian limits [72,73]. While this will become the practice as quantum lattice simulations become a precision endeavor, for now quantum noise and low shot rates dominate the error budget of calculations [74–76], burying errors from determining ξ. Thus, the idea of perturbative calculations of ξ becomes attractive, as it directly gives a fixed ξ trajectory in terms of the bare parameters. This implies that only the measurement of the spatial lattice spacing a through Euclidean simulation is required—reducing the classical computing resources. Through analytical continuation to Minkowski spacetime, spatial (temporal) spacings, a (a_t), are determined for quantum simulations [70].

In this paper, we perform the one-loop perturbative calculation of ξ using the background field method [77–80]. In the early days of lattice QCD, this technique along with other methods [81,82] were used to compute the scale parameter Λ [83,84], high-energy scattering [85]. Of relevance to quantum simulations, this included matching isotropic $3+1d$ $SU(N)$ lattice results to the Hamiltonian limit ($\xi \to \infty$) [86]. Later, this was extended to arbitrary anisotropy [87] and to the Hamiltonian limit in $2+1d$ [88]. Here, we present a unified derivation of ξ for $U(N)$ and $SU(N)$ for arbitrary dimensions and anisotropy. We will focus on the Wilson action and consider its connection to the Kogut-Susskind Hamiltonian. Similar studies can be carried out for quantum simulations of improved Hamiltonians [58–60] following initial work in $3+1d$ $SU(N)$ [89–93]. Since continuous gauge theories can be digitized for quantum simulations with discrete subgroups, we further explore whether our perturbative calculations for the continuous group can predict discrete subgroup results.

This paper is organized as follows. In Sec. II, we review the background field method and show how to perturbatively compute the renormalized anisotropy. This is followed by Sec. III and Sec. IV where the special cases of $U(1)$ and $SU(N)$ respectively are investigated. We extend the calculations to $U(N)$ in Sec. V. The anisotropy factors computed perturbatively are compared with Monte Carlo results for continuous and discrete groups in Sec. VI, to demonstrate the effectiveness of our perturbative computations. We leave Sec. VII to conclude and discuss future work. Details about the integrals involved in the perturbative calculations are in the Appendices.

II. BACKGROUND FIELD METHOD

Euclidean anisotropic lattices are characterized by the anisotropy $\xi = a/a_\tau$. Throughout this work, we will use Greek indices (μ, ν) to indicate spacetime dimensions, and Latin indices (i, j) to indication spatial dimensions. Consider the anistropic Wilson action:

$$S(U) = \sum_x \left[\beta_\sigma \sum_{i>j} \mathrm{Re\,Tr} P_{ij} + \beta_\tau \sum_i \mathrm{Re\,Tr} P_{0i} \right], \quad (1)$$

with the plaquette term

$$P_{\mu\nu} = \mathbb{1} - U_{x,x+\mu} U_{x+\mu,x+\mu+\nu} U^\dagger_{x+\nu,x+\mu+\nu} U^\dagger_{x,x+\nu}. \quad (2)$$

The two couplings in Eq. (1) are necessary in order to keep physics unchanged under independent variations of a and ξ. They are parametrized as

$$\beta_\sigma = \frac{z}{g^2_\sigma(a,\xi)} \xi^{-1} \quad \text{and} \quad \beta_\tau = \frac{z}{g^2_\tau(a,\xi)} \xi. \quad (3)$$

We will use $z = 2$ for $SU(N)$ and $U(N)$ groups, and $z = 1$ for $U(1)$ to ensure the canonical kinetic term in the continuum limit. The speed of light is defined as $c = g_\sigma/g_\tau$. We will denote the two couplings as g_μ, with $g_\mu = g_\sigma(g_\tau)$ for μ in the spatial direction (temporal direction). In the weak-coupling limit, the $g_\mu(a,\xi)$ can be expanded in terms of the isotropic value $\beta = z g_E^{-2}(a)$ as

$$\frac{1}{g^2_\mu(a,\xi)} = \frac{1}{g^2_E(a)} + c_\mu(\xi) + \mathcal{O}(g^2_E, \xi) \quad (4)$$

and $\xi = 1$ returns the usual isotropic formulation of a lattice gauge theory with $g_\sigma = g_\tau = g_E$. In the weak-coupling regime, the speed of light is given by

$$c = \frac{g_\sigma(a,\xi)}{g_\tau(a,\xi)}. \quad (5)$$

In a more symmetric fashion, the action of Eq. (1) can also be rewritten as

$$S(U) = \frac{z}{g^2_\xi} \sum_x \left[\bar{\xi}^{-1} \sum_{i>j} \mathrm{Re\,Tr} P_{ij} + \bar{\xi} \sum_i \mathrm{Re\,Tr} P_{0i} \right], \quad (6)$$

where the bare couplings $g^2_\xi = g_\sigma g_\tau \equiv z/\beta_\xi$ and the bare anisotropy $\bar{\xi} = c\xi$ are introduced; for every (a,ξ) pair there is a corresponding pair of bare couplings $(\beta_\xi, \bar{\xi})$. Following Eq. (4), we have

$$\frac{1}{g^2_\xi} \approx \frac{1}{g^2_E(a)} + \frac{c_\tau(\xi) + c_\sigma(\xi)}{2}. \quad (7)$$

The functions $c_\tau(\xi)$ and $c_\sigma(\xi)$ can be found by calculating the effective action $S^{(\xi)}_{\mathrm{eff}}$ of the lattice gauge theory for the two different lattice regularization procedures with $\xi = 1$ and $\xi \neq 1$. Requiring that in the continuum limit the effective action is independent of regularization, we have

$$\Delta S_{\text{eff}} = S_{\text{eff}}^{(\xi=1)} - S_{\text{eff}}^{(\xi\neq 1)} = 0. \tag{8}$$

This leads to the determination of $c_\tau(\xi)$ and $c_\sigma(\xi)$. The effective action can be perturbatively calculated using the background field method on the lattice [83].

We will denote $B_\mu(x)$ as the background field that solves the classical lattice equation of motion. With the fluctuating field α_μ, the lattice gauge variables can be parametrized as

$$\begin{aligned} U_{x,x+\mu} &= e^{iug_E a_\mu \alpha_\mu(x)} U^{(0)}_{x,x+\mu}, \\ U^{(0)}_{x,x+\mu} &= e^{iua_\mu B_\mu(x)}. \end{aligned} \tag{9}$$

For general dimensions, the couplings and fields may not be dimensionless, thus we rescale the couplings by a factor of $u = a^{D/2-2}$. Note that for one-loop calculations, we can use the isotropic coupling g_E in these exponents instead of g_μ. The covariant derivatives are defined as

$$\begin{aligned} D_\mu f(x) &= \frac{1}{a_\mu}(U_{x,x+\mu} f(x+\mu) U^\dagger_{x,x+\mu} - f(x)), \\ \bar{D}_\mu f(x) &= \frac{1}{a_\mu}(U^\dagger_{x-\mu,x} f(x-\mu) U_{x-\mu,x} - f(x)). \end{aligned} \tag{10}$$

The lattice derivatives $\Delta_\mu f(x)$ and $\bar{\Delta}_\mu f(x)$ follow from Eq. (10) by setting $U_{x,x+\mu} = \mathbb{1}$. Taking $U_{x,x+\mu} \to U^{(0)}_{x,x+\mu}$ defines $D^{(0)}_\mu f(x)$, $\bar{D}^{(0)}_\mu f(x)$. The lattice action can be expanded around $U_{x,x+\mu} = U^{(0)}_{x,x+\mu}$ as

$$S(U) = S_0 + S_2 + \cdots, \tag{11}$$

where $S_0 = S(U^{(0)})$ and S_2 includes terms quadratic in α_μ. To preserve the gauge symmetry of the background field, we work in the background Feynman gauge [94] which requires adding the gauge-fixing term

$$S_{\text{gf}} = a^{D-1} a_\tau \sum_x \text{Tr}\left(\sum_\mu \bar{D}^{(0)}_\mu \alpha_\mu(x)\right)^2 \tag{12}$$

and an associated ghost term $S_{\text{gh}}(\phi)$ for a ghost field ϕ when a non-Abelian gauge theory is considered:

$$S_{\text{gh}} = 2a^{D-1} a_\tau \sum_{x,\mu} \text{Tr}[(D^{(0)}_\mu \phi(x))^\dagger (D^{(0)}_\mu \phi(x))]. \tag{13}$$

The partition function can be calculated as

$$\begin{aligned} Z &\equiv \int [dU] e^{-S(U)} \\ &\approx e^{-S_0} \int [d\alpha][d\phi] e^{-(S_2 + S_{\text{gf}} + S_{\text{gh}})}(1 + \mathcal{O}(g_E^2)) \\ &\approx e^{-S_0} \int [d\phi] e^{-S_{\text{gh}}} \int [d\alpha] e^{-S_{\text{free}}} e^{-S'_2} \\ &\approx \int [d\phi] e^{-S_{\text{gh}}} \int [d\alpha] e^{-S_{\text{free}}} \left(1 - S_0 - S'_2 + \frac{S'^2_2}{2} + \cdots\right) \\ &\propto e^{-S^{(\xi)}_{\text{eff}}} \approx 1 - S^{(\xi)}_{\text{eff}} + \cdots, \end{aligned} \tag{14}$$

where we have extracted the free action S_{free} for the fluctuating field α_μ from $S_2 + S_{\text{gf}}$ and denote the rest as S'_2. On the fourth line, we have Taylor expanded $e^{-S_0 - S'_2}$.

In this article, we consider the $F^2_{\mu\nu}$ term in $S_{\text{eff}}(\xi)$ at one loop. This gives the $\mathcal{O}(g_E^0)$ corrections $c_\tau(\xi)$ and $c_\sigma(\xi)$. Matching terms in Eq. (14) we see $S^{(\xi)}_{\text{eff}}$ is related to expectation values computed with respect to S_{free}:

$$S^{(\xi)}_{\text{eff}} = S_0 + \langle S'_2 \rangle - \frac{1}{2}\langle S'^2_2 \rangle + \langle S_{\text{gh}} \rangle_\phi. \tag{15}$$

Similarly, the contributions from S_{gh} can be calculated as $\langle S_{\text{gh}} \rangle_\phi$. Higher loop corrections carry additional factors of the coupling g_E^2 and are negligible at weak coupling.

III. $U(1)$ GAUGE THEORY

We apply the background field methods to $U(N)$ and $SU(N)$ to compute the perturbative relations for Euclidean lattices at any anisotropy and in any dimension. We will initially consider the simpler $U(1)$ gauge theory, then consider the more involved case of $SU(N)$ gauge theory, followed by the $U(N)$ gauge theory.

For the $U(1)$ gauge theory, B_μ and α_μ are the single component electromagnetic fields and we can trivially perform the traces in Eq. (12) to find

$$S_{\text{gf}} = \frac{1}{2} a^{D-1} a_\tau \sum_x \left(\sum_\mu \bar{D}^{(0)}_\mu \alpha_\mu(x)\right)^2, \tag{16}$$

while the S_{free} is found to be

$$S_{\text{free}} = \frac{1}{2} a^{D-1} a_\tau \sum_{x,\mu,\nu} (\Delta_\mu \alpha_\nu)(\Delta_\mu \alpha_\nu), \tag{17}$$

and S'_2 is given by

$$S'_2 = -\frac{a^{2D-5} a_\tau}{8} \sum_{x,\mu,\nu,a} (a_\mu a_\nu F_{\mu\nu})^2 (\Delta_\mu \alpha_\nu - \Delta_\nu \alpha_\mu)^2. \tag{18}$$

The nonvanishing contributions to Eq. (15) are given by

$$S_{\text{eff}}^{(\xi)} = S_0 + \langle S_2' \rangle, \tag{19}$$

where in $U(1)$ we can neglect the $\langle S_2'^2 \rangle$ term as it only contributes to higher orders of $F_{\mu\nu}^2$. Further, the ghost term is zero in $U(1)$. $S_{\text{eff}}^{(\xi)}$ for $U(1)$ in arbitrary dimensions can then be written as

$$S_{\text{eff}}^{(\xi)} = \frac{1}{4}\int d^D x \left(\sum_i [(F_{i0}^a)^2 + (F_{0i}^a)^2][g_\tau^{-2} - f_\tau(\xi)] + \sum_{i,k} (F_{ik}^a)^2 [g_\sigma^{-2} - f_\sigma(\xi)] \right) \tag{20}$$

with

$$f_\tau(\xi) = \frac{1}{2\xi}\left(1 - \frac{D-2}{D-1}\xi^{-1} I_1(\xi)\right),$$
$$f_\sigma(\xi) = \frac{I_1(\xi)}{D-1}. \tag{21}$$

$I_1(\xi)$ and other integrals required for this paper are defined in Appendix A, following [87]. One can show $I_1(1) = \frac{D-1}{D}$ and $f_\tau(\xi \to \infty) = 0$. For $\xi = 1$, both $f_\mu(1) = 1/D$ and thus $g_E^2(\text{one-loop}) = g_E^2[1 + f_\tau(1)] = g_E^2[1 + 1/D]$ which agrees with previous $D = 4$ calculations [95]. From $f_\mu(\xi)$, we obtain

$$c_\mu(\xi) = f_\mu(\xi) - f_\mu(\xi = 1). \tag{22}$$

These functions are shown in Fig. 1 for 3 and 4 dimensions. In the $\xi \to \infty$ limit, we show in Appendix B that

$$I_1(\xi \to \infty) \approx \sqrt{\frac{D-1}{2} - \frac{1}{16}} \tag{23}$$

and that $c_\tau(\xi \to \infty) = -1/D$. Specific numerical values when $D = 3$, 4 are

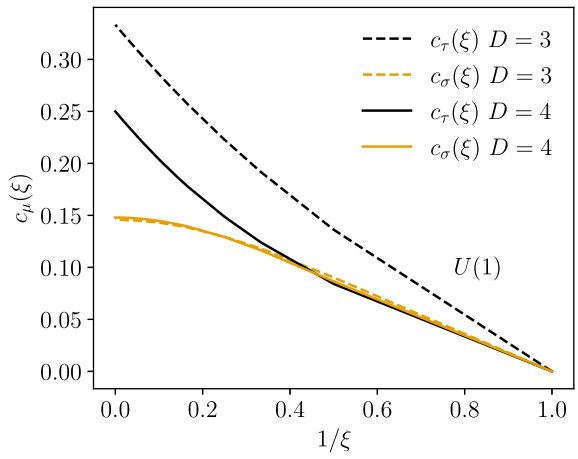

FIG. 1. Anisotropic coefficients for $U(1)$ in $D = 3$, 4.

$$c_\tau(\xi \to \infty) = -\frac{1}{3}, -\frac{1}{4} \quad (D = 3, 4),$$
$$c_\sigma(\xi \to \infty) = 0.146, 0.148 \quad (D = 3, 4). \tag{24}$$

IV. $SU(N)$ GAUGE THEORY

We now move to consider the more complicated case of $SU(N)$. B_μ and α_μ can be expanded in terms of the group generators $\lambda^a, a = 1, \ldots, N^2 - 1$:

$$B_\mu = B_\mu^a \lambda^a/2, \qquad \alpha_\mu = \alpha_\mu^a \lambda^a/2, \tag{25}$$

with the generators normalized to $\text{Tr}\lambda^a\lambda^b = 2\delta_{ab}$. Using the gauge-fixing term in Eq. (12) and the ghost term in Eq. (13), we can rewrite $S_2 + S_{\text{gf}}$ in terms of a tensor S_T, a scalar S_{sc} and two vector interactions S_A and S_B:

$$S_T = -\frac{a^{2D-5}a_\tau}{8N}\sum_{x,\mu,\nu,a}(a_\mu a_\nu F_{\mu\nu}^a)^2 \text{Tr}(\Delta_\mu\alpha_\nu - \Delta_\nu\alpha_\mu)^2,$$
$$S_{\text{sc}} = a^{D-1}a_\tau \sum_{x,\mu,\nu}\text{Tr}[(D_\mu^{(0)}\alpha_\nu)(D_\mu^{(0)}\alpha_\nu)],$$
$$S_A = a^{D-1}a_\tau \sum_{x,\mu\nu} a^{(D-4)/2}\text{Tr}(A_{\mu\nu}(x)F_{\mu\nu}(x)),$$
$$S_B = \frac{1}{2}a^{D-1}a_\tau \sum_{x,\mu,\nu} a^{(D-4)/2}\text{Tr}(B_{\mu\nu}(x)F_{\mu\nu}(x)). \tag{26}$$

$A_{\mu\nu}(x)$ and $B_{\mu\nu}(x)$ are antisymmetric and symmetric in the vector indices, respectively, and given by

$$A_{\mu\nu}(x) = -i\Big\{2[\alpha_\nu, \alpha_\mu] + a_\nu[\alpha_\nu, D_\nu^{(0)}\alpha_\mu] + a_\mu[D_\mu^{(0)}\alpha_\nu, \alpha_\mu] + \frac{a_\mu a_\nu}{2}[D_\mu^{(0)}\alpha_\nu, D_\nu^{(0)}\alpha_\mu]\Big\}$$
$$B_{\mu\nu}(x) = -i(a_\mu[D_\nu^{(0)}\alpha^\mu, \alpha^\mu] + a_\nu[\alpha^\nu, D_\mu^{(0)}\alpha^\nu]). \tag{27}$$

From S_{sc}, we extract the free action for the α_μ field:

$$S_{\text{free}} = a^{D-1}a_\tau \sum_{x,\mu,\nu}\text{Tr}[(\Delta_\mu\alpha_\nu)(\Delta_\mu\alpha_\nu)] \tag{28}$$

and define $S_{\text{sc,I}} = S_{\text{sc}} - S_{\text{free}}$. The nonvanishing contributions to the effective action are given by

$$S_{\text{eff}}^{(\xi)} = S_0 + \langle S_T\rangle - \frac{1}{2}\langle S_A^2\rangle - \frac{1}{2}\langle S_B^2\rangle + \frac{D-2}{D}\left[\langle S_{\text{sc},I}\rangle - \frac{1}{2}\langle S_{\text{sc},I}^2\rangle\right] \tag{29}$$

with other terms vanishing. Notice that unlike $U(1)$, $\langle S_2^2\rangle$ terms contribute at leading order. The factor $\frac{D-2}{D}$ comes from the fact that the ghost field contribution cancels 2 out

of D degrees of freedom of α_μ. Where again the expectation values are calculated with respect to S_{free}. The final one-loop corrected action is given by

$$S_{\text{eff}}^{(\xi)} = \frac{1}{4}\int d^D x \Bigg(\sum_i [(F_{i0}^a)^2 + (F_{0i}^a)^2][g_\tau^{-2} - f_\tau(\xi)] + \sum_{i,k} (F_{ik}^a)^2 [g_\sigma^{-2} - f_\sigma(\xi)] \Bigg). \tag{30}$$

$SU(N)$, $f_\mu(\xi)$ are defined as

$$\begin{aligned} f_\tau(\xi) &= 4N\left[\frac{N^2-1}{16N^2}\left\{\frac{\xi^{-2} I_1(\xi)}{(D-1)} + \xi^{-1} I_5(\xi)\right\} + \frac{1}{64} I_{2b}(\xi) \right. \\ &\quad + \frac{D-14}{384(D-1)} I_{2a}(\xi) + \frac{1}{256} I_4(\xi)\xi^{-2} + \frac{D-8}{192}\xi^{-2} I_6(\xi) \\ &\quad \left. + \frac{2-D}{384}\xi^{-2} I_7(\xi) + \frac{26-D}{24}\text{DIV}(\xi)\right], \\ f_\sigma(\xi) &= 4N\left[\frac{N^2-1}{8N^2}\frac{I_1(\xi)}{(D-1)} + \frac{D-14}{192(D-1)} I_{2a}(\xi) \right. \\ &\quad \left. + \frac{8-D}{192} I_3(\xi) + \frac{1}{128} I_4(\xi) + \frac{26-D}{24}\text{DIV}(\xi)\right]. \end{aligned} \tag{31}$$

The DIV part defined as

$$\text{DIV}(\xi) = \frac{2^{D-4}}{(2\pi)^D}\int_{-\pi/2}^{\pi/2} d^{D-1}x \int_{(-\pi/2)\xi}^{(\pi/2)\xi} dx_0 \times \left(\sum_{i=1}^{D-1} \sin^2 x_i + \xi^2 \sin^2(x_0/\xi)\right)^{-2}, \tag{32}$$

is divergent. This divergence comes from S_A and $S_{\text{sc,I}}$ terms which do have corresponding continuum limit and contain logarithmic divergence as $a \to 0$. With the definition for $c_\mu(\xi)$ in Eq. (22), the divergence part in DIV(ξ) are subtracted out. Our calculation gives the same results as [87] for $D = 4$ and as [86,88] in the $\xi \to \infty$ limit. The values of $c_\mu(\xi)$ for $SU(3)$ gauge theory are shown in Fig. 2 at different dimensions.

V. $U(N)$ GAUGE THEORY

The Lie algebra for $U(N)$ group can be constructed by introducing the additional generator $\lambda^0 = \sqrt{\frac{2}{N}}\mathbb{I}_{N\times N}$ to the $SU(N)$ group. Corresponding to any index a for $SU(N)$ group we introduce the index $A = (0, a)$, so that A runs from 0 to $N^2 - 1$. With this construction, we still have $\text{Tr}[\lambda^A \lambda^B] = 2\delta_{AB}$; special care has to be taken for the anti-symmetric structure constant as $f_{0BC} = 0$. The final one-loop corrected action is given by

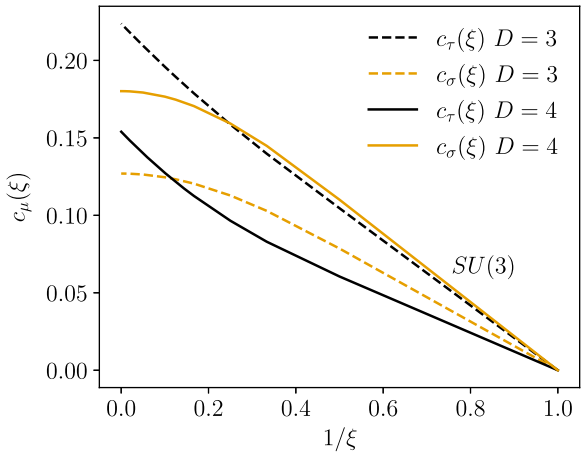

FIG. 2. Anisotropic coefficients for $SU(3)$ in $D = 3$, 4.

$$\begin{aligned} S_{\text{eff}}^{(\xi)} = \frac{1}{4}\int d^D x \Bigg(& \sum_i [(F_{i0}^a)^2 + (F_{0i}^a)^2][g_\tau^{-2} - f_\tau(\xi)] \\ & + \sum_{i,k} (F_{ik}^a)^2 [g_\sigma^{-2} - f_\sigma(\xi)] \\ & + \sum_i [(F_{i0}^0)^2 + (F_{0i}^0)^2][g_\tau^{-2} - f_{0,\tau}(\xi)] \\ & + \sum_{i,k} (F_{ik}^0)^2 [g_\sigma^{-2} - f_{0,\sigma}(\xi)] \Bigg), \end{aligned} \tag{33}$$

with $f_\tau(\xi)$ and $f_\sigma(\xi)$ given by Eq. (31) but replacing $N^2 - 1$ by N^2 which changes the factor $\frac{N^2-1}{N^2}$ to 1, and $f_{0,\tau}(\xi)$ and $f_{0,\sigma}(\xi)$ corresponding to Eq. (21) multiplied by a factor of $N/2$.

VI. COMPARING TO NUMERICAL RESULTS

Our values of c_σ and c_τ computed in Secs. III and IV can be used to calculate the renormalized anisotropy, ξ using the relation $\bar{\xi} = c\xi$, with c given in Eq. (5) and expressions for g_μ in Eq. (4). In this section, we compare our one-loop calculations of ξ as well as the bare anisotropy with nonperturbative results obtained from two sets of Monte Carlo results. The first are existing $2+1$d $U(1)$ and $SU(2)$ results produced in Refs. [96,97]. The second are new ensembles produced by us for the discrete cyclic groups $\mathbb{Z}_{10}$ and $\mathbb{Z}_{100}$, and the binary icosahedral ($\mathbb{BI}$). These discrete groups are of interest because they are subgroups of $U(1)$ and $SU(2)$, respectively, and have been proposed as approximations for use on quantum computers. Thus, it is interesting to investigate how well perturbative lattice field theory for the continuous group can approximate ξ for the discrete subgroups. In both previous works, smearing was used to reduce the need for higher statistics. This has the consequence of changing the lattice spacings by a unknown, potentially large amount and can introduce some discrepancy between the

perturbative and the nonperturbative results. For this reason, in our simulations we avoided using smearing at the cost of a larger number of lattice configurations.

The discrete group ensembles were generated by sampling from the Wilson action using a multi-hit Metropolis update algorithm, which has been found to be as efficient as a heat-bath in terms of autocorrelation length but significantly cheaper to implement for discrete groups [6]. The various ensemble parameters are found in Table I. Using discrete groups, we must worry about crossing into the frozen phase where all the links take the value of group identity $\mathbb{1}$ at a critical coupling β_f for isotropic lattice. For $\mathbb{Z}_n$ groups, it is known that [98]

$$\beta_{f,n} \approx \frac{A}{1-\cos(\frac{2\pi}{n})}, \tag{34}$$

For $3+1d$ in [98], the theoretical value of A was obtained to be $A_{3\mathrm{d}}^{\mathrm{th}} \approx \log(1+\sqrt{2})$, while numerical simulations gave $A_{3\mathrm{d}} = 0.78$ [99,100]. For the case of $2+1d$, using the value $\beta_{f,2} = 0.761412$ obtained from Monte Carlo simulations in [101–103], the theoretical value of A is calculated following Eq. (34) to be $A_{2\mathrm{d}}^{\mathrm{th}} = 1.52282$. As a comparison, we compute $A_{2\mathrm{d}}$ with the following procedure. For certain n, we measure the average plaquette energy $\langle E\rangle$ as a function of β. $\beta_{f,n}$ is determined as the β value that maximizes the specific heat $|\frac{\partial\langle E\rangle}{\partial\beta}|$. We compute $\beta_{f,n}$ for $n = 2, 3\ldots, 10$ on 10^3 lattices. As an example, we show the measured value of $\langle E\rangle$ in Fig. 3 for $n = 10$ at different β values. Fitting the $\beta_{f,n}$ values to Eq. (34), we obtain $A_{2\mathrm{d}} = 1.450(12)$. Two additional $\beta_{f,n}$ for $n = 12$, 15 are computed and they agree well with the fit. These results are plotted in Fig. 4. Comparing to the $A_{2\mathrm{d}}^{\mathrm{th}}$, we expect that corrections to the theoretical value are needed.

TABLE I. Ensemble parameters for the lattice simulations: Group G, coupling β, bare anisotropy $\bar{\xi}$, Lattice dimensions $N_s^D \times N_t$, decorrelation length n_{decor} and number of configurations n_{meas}.

G	β	$\bar{\xi}$	$N_s^D \times N_t$	n_{decor}	n_{meas}
$\mathbb{Z}_{10}$, $\mathbb{Z}_{100}$	1.35	2.25	$16^2 \times 48$	10	8×10^6
$\mathbb{Z}_{10}$, $\mathbb{Z}_{100}$	1.35	2.25	$24^2 \times 72$	10	4×10^6
$\mathbb{Z}_{10}$, $\mathbb{Z}_{100}$	1.55	2.5	$16^2 \times 48$	10	5×10^6
$\mathbb{Z}_{10}$, $\mathbb{Z}_{100}$	1.55	2.5	$24^2 \times 72$	10	1×10^6
$\mathbb{Z}_{10}$, $\mathbb{Z}_{100}$	1.7	3.0	$16^2 \times 48$	10	5×10^6
$\mathbb{Z}_{10}$, $\mathbb{Z}_{100}$	1.7	3.0	$20^2 \times 60$	10	5×10^6
$\mathbb{Z}_{10}$, $\mathbb{Z}_{100}$	1.7	3.0	$24^2 \times 72$	10	1×10^6
$\mathbb{Z}_{10}$, $\mathbb{Z}_{100}$	2.0	3.0	$16^2 \times 48$	10	5×10^6
$\mathbb{Z}_{10}$, $\mathbb{Z}_{100}$	2.0	3.0	$20^2 \times 60$	10	5×10^6
$\mathbb{Z}_{10}$, $\mathbb{Z}_{100}$	2.0	3.0	$24^2 \times 72$	10	1×10^6
$\mathbb{BI}$	2.0	2.0	$36^2 \times 72$	10	5000
$\mathbb{BI}$	3.0	1.33	$36^2 \times 72$	10	5000
$\mathbb{BI}$	3.0	1.33	$36^3 \times 72$	10	250

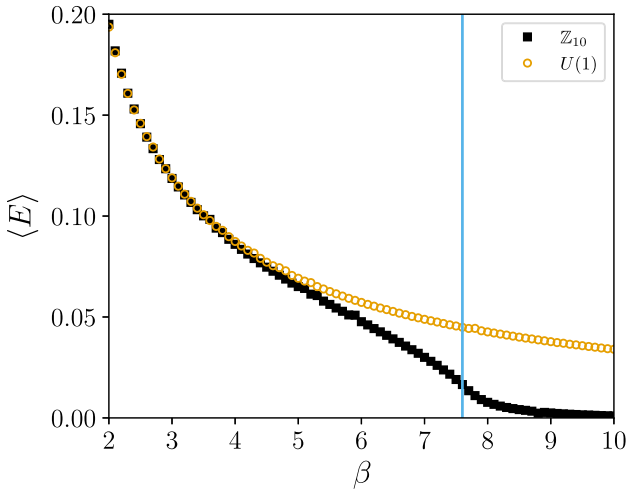

FIG. 3. Average plaquette energy $\langle E\rangle$ as a function of β for Z_{10} and $U(1)$, with $\beta_{f,10} = 7.6$ indicated by the vertical line.

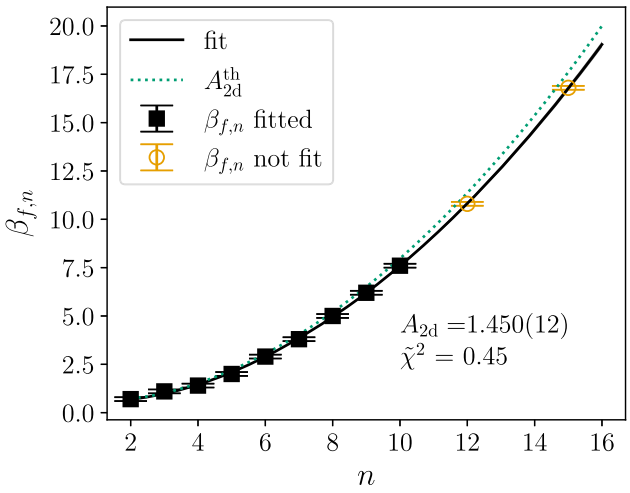

FIG. 4. $\beta_{f,n}$ versus n. $\mathbb{Z}_n$ for $n \leq 10$ (black square) were used to perform the fix, while $n > 10$ to test the extrapolation.

In the case of anisotropic lattices considered here, one should expect the effects of the freezing-out to occur when $\beta_\xi\bar{\xi} = \beta_{\xi,f}\bar{\xi} \approx \beta_f$. However, as we observe, for isotropic lattice, $\mathbb{Z}_{10}$ deviates from $U(1)$ around $\beta \approx 5$ which is much smaller than $\beta_{f,10} = 7.6$ (See Fig. 3). Hence, we expect that $\beta_\xi\bar{\xi} \ll \beta_f$ is necessary to ensure discrete subgroups being a reasonable approximation in $2+1d$. In $3+1d$, deviations occur at β values relatively closer to β_f compared to $2+1d$, as observed in [6,104]. To compare with existing nonperturbative results for $U(1)$ in $2+1d$ studied by Loan *et al.* [96], we generate ensembles for $\mathbb{Z}_{10}$ and $\mathbb{Z}_{100}$ groups at the same set of $(\beta_\xi, \bar{\xi})$ used by them (see Table II). The two largest pairs investigated in [96] are $\beta_\xi\bar{\xi} = 1.7 \times 3.0 = 5.1$ and $\beta_\xi\bar{\xi} = 2.0 \times 3.0 = 6.0$, not much smaller than $\beta_{f,10}$, and therefore we expect to observe breakdown of the agreement between $\mathbb{Z}_{10}$ and the $U(1)$

results. In contrast, $\beta_{f,100} > 700$ so $\mathbb{Z}_{100}$ results should be indistinguishable from a equivalent $U(1)$ computation.

The results of $2+1$d $SU(2)$ from [97] consider $\beta_\xi\bar{\xi}$ (see Table III) above or too close to $\beta_{f,\mathbb{BI}} = 9.65(1)$ that we calculated by similar procedures described above. Hence in the following we will not make direct comparisons between discrete groups and continuous groups, but instead compare the viability of the one-loop calculations with the $SU(2)$ continuous group. Then we computed $\mathbb{BI}$ configurations at different values where $\beta_\xi\bar{\xi} = 4$ and compare those results with our one-loop calculations. Additionally, we performed one simulation of $3+1$d $\mathbb{BI}$ and also compare with our one-loop calculations.

Different methods are available for determining ξ from lattice results. Loan *et al.* [96] utilized the ratio of subtracted static potentials, where a subtraction point must be picked. Teper *et al.* [97] uses two methods: the first compares correlators in the spatial and temporal direction which can also be used to determine ξ in real-time simulations [70], the second computes the dispersion relation with low-lying momentum states and tunes ξ to obtain $E(p) \approx \sqrt{m_P^2 + p^2}$. These two results are then averaged to obtain a final estimate of ξ.

We determined ξ for the discrete groups via the "ratio-of-ratios" method [105]. This method involves computing the ratios of Wilson loops:

$$R_{ss}(x,y) = \frac{W_{ss}(x,y)}{W_{ss}(x+1,y)}, \qquad R_{st}(x,t) = \frac{W_{st}(x,t)}{W_{st}(x+1,t)}, \tag{35}$$

where x, y, t are the integer lattice separations and the subscripts indicate the orientation of the Wilson loops, either spatial spatial, or spatial temporal. In the large x limit where the excited state contamination is suppressed, we have $W_{ss}(x,y) \propto e^{-axV_s(ya)}$ and $W_{st}(x,t) \propto e^{-axV_s(ta_\tau)}$ with V_s being the static quark-antiquark potential. This lead to

$$R_{ss}(x,y)|_{x\to\infty} = e^{-aV_s(ya)}, \tag{36}$$

$$R_{st}(x,t)|_{x\to\infty} = e^{-aV_s(ta_\tau)}. \tag{37}$$

We define a variable

$$\delta(x,y,t) = \frac{R_{ss}(x,y)}{R_{st}(x,t)} - 1, \tag{38}$$

such that $\delta(x,y,t) = 0$ will be satisfied in the large x limit when $ya = ta_\tau$. We determine $\xi(y) = t/y$. Figure 5 (top) shows the plateau behavior of $\delta(x,y,t)$ when we approach the large x limit. Typically, the zero crossing does not occur for integer y, t and thus interpolation between values is required. An example of this calculation is shown in Fig. 5 (bottom) for $\mathbb{Z}_{100}$ using $y = 3$, $\beta_\xi = 1.7$, and $\bar{\xi} = 3.0$ on a lattice of size $N_s^D \times N_t = 20^2 \times 60$. The final step is to take the $\xi(y)$ value in the large y limit as our renormalized ξ, to again remove excited states contamination (see Fig. 6). The increasing uncertainty at larger y is due to exponential decay of the Wilson loop $W_{ss}(x,y)$ leading to a signal-to-noise problem.

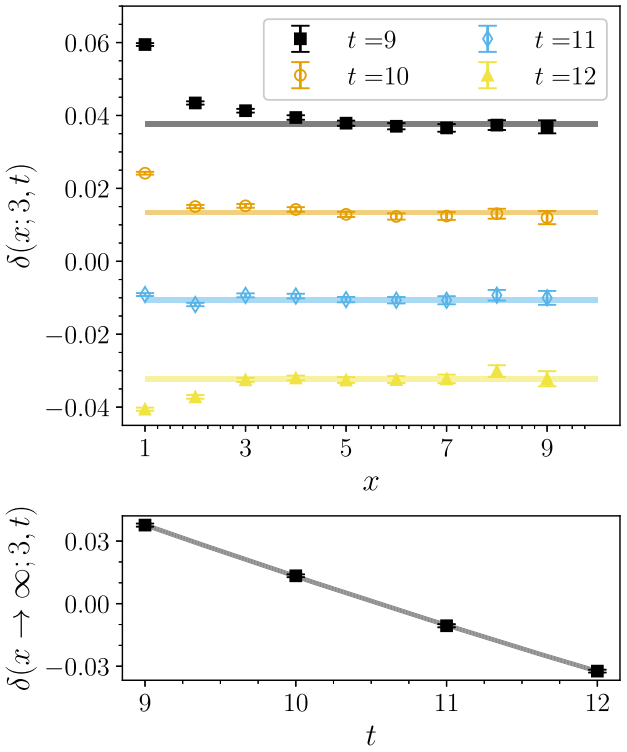

FIG. 5. Example calculations of $\delta(x;y,t)$ for $y = 3$ as a function of x (top), $\delta(x \to \infty, 3, t)$ for various values of t (bottom) fitted to determine $\delta(x \to \infty, y; t) = 0$, for $\mathbb{Z}_{100}$ using $\beta_\xi = 1.7$, and $\bar{\xi} = 3.0$ on a lattice of size $N_s^D \times N_t = 20^2 \times 60$.

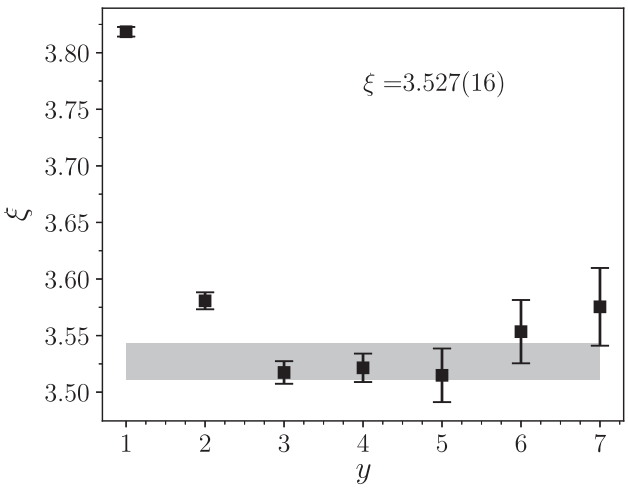

FIG. 6. Measured ξ as a function of y. The band corresponds to the 1σ error band for best fit to the plateau region. The ensemble parameters are the same as for Fig. 5.

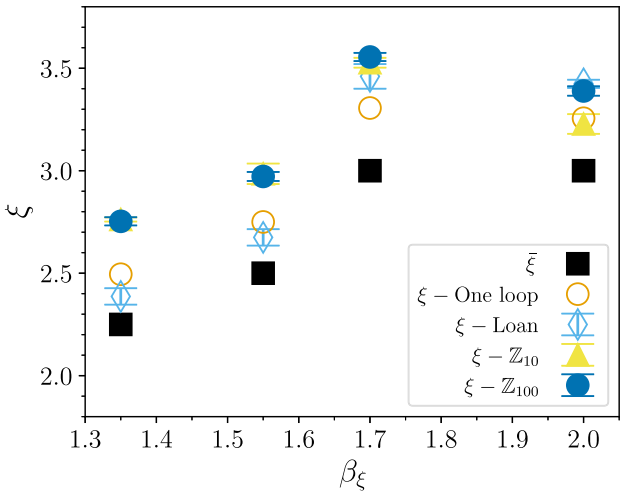

FIG. 7. Comparison of one-loop ξ to $\bar{\xi}$, the nonperturbative ξ value from Loan *et al.* ($r_0 = \sqrt{2}$) [96] for $2+1d$ $U(1)$ theory, and for $\mathbb{Z}_n$ discrete group.

In Fig. 7, we show the comparisons between the ξ values from our one-loop calculation to the results from nonperturbative Monte Carlo simulation from Loan *et al.* [96] for $U(1)$ gauge theory in $2+1d$, alongside with our results for $\mathbb{Z}_{10}$ and $\mathbb{Z}_{100}$ also in $2+1d$. It is encouraging to see that including one-loop effects shifts ξ into better agreement with the nonperturbative results compared to $\bar{\xi}$. As a metric for comparison, we use the relative errors

$$\mathcal{F}_g = \left|1 - \frac{\xi_{1-\text{loop}}}{\xi_g}\right|,$$
$$\mathcal{F}_g^{\bar{\xi}} = \left|1 - \frac{\bar{\xi}}{\xi_g}\right|, \tag{39}$$

where g is the nonperturbative data to which we are comparing our one loop results. For the smeared results for $U(1)$, we find $\mathcal{F}_{U(1)} \leq 4.71(8)\%$ compared to $\mathcal{F}^{\bar{\xi}}_{U(1)} \leq 13.3(15)\%$.

The situation with $\mathbb{Z}_n$ is more involved. For $\beta_\xi < 1.65$, we find that $\xi_{\mathbb{Z}_{10}} = \xi_{\mathbb{Z}_{100}}$ but are systematically higher than the $U(1)$ results. At present, we do not understand why at lower β_ξ greater disagreement is found between the discrete and continuous groups, since lower values of β_ξ are further from the freezing-out regime and they should be in better agreement. We investigated whether finite volume effects could be playing a role, but for all values of $\{\beta_\xi, \bar{\xi}\}$, we observed no volume dependence, as seen in Tables II and III. Two possible sources of the discrepancy could be the use of smearing in [96,97] or the different methods of measuring ξ. Future work should be undertaken where the discrete and continuous groups are analyzed under the same circumstances. As β_ξ increases, $\xi_{\mathbb{Z}_{100}}$ approaches $\xi_{U(1)}$, with $\mathbb{Z}_{10}$ having noticeable and growing disagreement. Across β, we found $\mathcal{F}_{\mathbb{Z}_{10}} \approx \mathcal{F}_{\mathbb{Z}_{100}} \leq 9.5(3)\%$ compared to $\mathcal{F}^{\bar{\xi}}_{\mathbb{Z}_{10},\mathbb{Z}_{100}} \leq 18.5(3)\%$. Higher order loop corrections, of $\mathcal{O}(g_E^4)$ to the ξ could be important for the β_ξ regions considered and effects of monopoles may also be relevant [95].

TABLE II. Renormalized anisotropies of $U(1)$ from 1-loop calculation, lattice simulations of $\mathbb{Z}_{10}$ and $\mathbb{Z}_{100}$, and $U(1)$ [96].

					ξ		
β_ξ	N_s	N_t	$\bar{\xi}$	$\xi_{1-\text{loop}}$	$\mathbb{Z}_{10}$	$\mathbb{Z}_{100}$	$U(1)$ [96]
1.35	16	48	2.25	2.493	2.738(20)	2.732(30)	2.39(4)
1.35	24	72	2.25	2.493	2.762(10)	2.753(20)	⋯
1.55	16	48	2.50	2.750	2.939(29)	2.972(40)	2.72(9)
1.55	24	72	2.50	2.750	2.984(50)	2.972(22)	⋯
1.70	16	48	3.00	3.302	3.513(11)	3.572(10)	3.46(6)
1.70	20	60	3.00	3.302	3.512(20)	3.527(16)	⋯
1.70	24	72	3.00	3.302	3.527(24)	3.555(20)	⋯
2.00	16	48	3.00	3.253	3.259(17)	3.421(15)	3.42(3)
2.00	20	60	3.00	3.253	3.252(38)	3.379(20)	⋯
2.00	24	72	3.00	3.253	3.228(48)	3.389(23)	⋯

TABLE III. Renormalized anisotropies from 1-loop calculation, discrete group $\mathbb{BI}$, and [97].

					ξ	
β_ξ	N_s	N_t	$\bar{\xi}$	$\xi_{1-\text{loop}}$	$\mathbb{BI}$	$SU(2)$ [97]
$D=3$						
2.00	36	72	2.00	2.097	2.099(1)	⋯
2.00	12[a]	60[a]	4.00	4.278	⋯	4.35(19)
2.65	16[a]	64[a]	4.00	4.207	⋯	4.22(11)
3.00	36	72	1.33	1.351	1.369(19)	⋯
4.00	24[a]	96[a]	4.00	4.136	⋯	4.08(9)
$D=4$						
3.0	36	72	1.33	1.351	1.36(1)	⋯

[a]This is the largest volume simulated.

We can also compare our $\xi_{1-\text{loop}}$ for $SU(2)$ in $2+1d$ to the results from nonperturbative Monte Carlo simulations [97], which are shown in Fig. 8 and Table III, and to the ξ values we computed for the $\mathbb{BI}$ group (Table III). The effect of the one-loop correction is to increase ξ by about 10%. The largest error from using $\bar{\xi}$ was found to be $\mathcal{F}^{\bar{\xi}}_{SU(2),\mathbb{BI}} \leq 8(4)\%$. In contrast, we observe $\mathcal{F}_{SU(2)} \leq 1(4)\%$ and $\mathcal{F}_{\mathbb{BI}} = 1.30(13)\%$ both consistent with 0—albeit the $SU(2)$ Monte Carlo results have larger uncertainties compared to the $U(1)$ case. This agreement is found in both $2+1d$ and $3+1d$ $\mathbb{BI}$ results (see Table III).

In all the groups studied, $\mathcal{F}_g$ was found to decrease or remain constant as β_ξ was increased—in agreement with expectation for a weak-coupling calculation, with the caveat that for discrete groups, β_ξ should be away from the freezing-out regime. For all the β_ξ values investigated here, we obtain that the systematic error of approximating the one loop results to the nonperturbative results for both

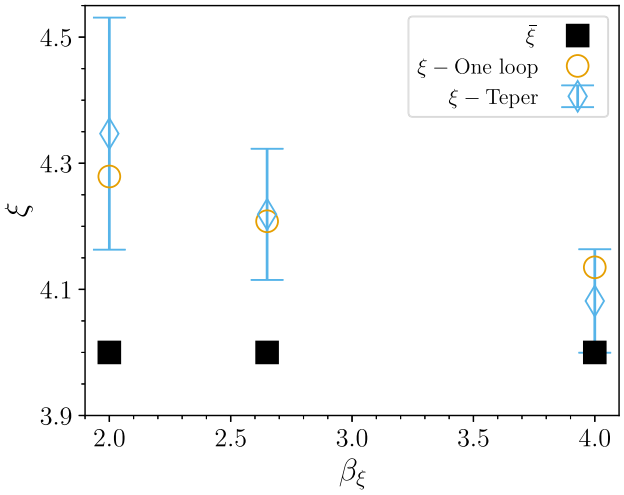

FIG. 8. Comparison of one-loop ξ to nonperturbative value of [97] for $2+1d$ $SU(2)$, with $\bar{\xi}=4$.

discrete group and continuous group is less than 10%. Given that these β_ξ values are corresponding to relative strong coupling, 10% systematic error are conservative for realistic simulations using quantum computers where larger β_ξ values are used.

VII. CONCLUSIONS

Quantum field theories simulated with quantum computers are naturally lattice-regularized theories, requiring renormalization before comparisons to experiments can be made. Quantum simulations are constructed within the Hamiltonian formalism, where a spatial lattice with spacing a is time evolved. Further approximations are required, as the time evolution operator $\mathcal{U}(t)$ built from the Kogut-Susskind Hamiltonian usually cannot be exactly implemented in an efficient manner. One common method for these approximations is trotterization, which introduces finite temporal lattice spacings a_t and thus a finite anisotropy factor a/a_t in the quantum simulations. As the trotterized $\mathcal{U}(t)$ can be related to the Euclidean transfer matrix on the anisotropic lattice via analytical continuation, it is thus beneficial to have the perturbative relations between the bare and renormalized quantities in Euclidean spacetime, e.g. the anisotropy factor ξ as a function of β_ξ and $\bar{\xi}$).

In the near term, studies of quantum field theory on quantum computing will be limited to low dimensions at coarse a_t. In this article, we extended the perturbative matching of coupling constants to general $SU(N)$ and $U(N)$ gauge theories for any anisotropy factor ξ and general dimensions. The results presented here can be easily used for Euclidean measurements as well as inputs to quantum simulations through analytical continuation. As examples, we compared anisotropy factors obtained via the one-loop renormalization to those determined from Monte Carlo simulations, and found great agreement for $SU(N)$ gauge theories. For $U(1)$ gauge theories, the one-loop calculation corrects most of the renormalization effects observed in the nonperturbative results. To the best of our knowledge, these comparisons were not previously performed before and provide important guidance for the validity of the perturbative calculations. Taken holistically, our results suggest that the one-loop ξ can serve as a replacement for the nonperturbative value in lattice calculations while inducing a systematic error $\lesssim 10\%$, with $SU(2)$ appearing to have better agreement than $U(1)$ in $2+1d$. In the weak coupling regime at sufficiently small a, this error is subleading to quantum errors for near term quantum simulations. Comparing the ξ parameters calculated perturbatively for continuous groups with those calculated nonperturbatively for discrete groups, we find satisfactory agreement, suggesting that the perturbative relations derived in this paper are also applicable to discrete groups in the parameter space of interest.

ACKNOWLEDGMENTS

This work is supported by the Department of Energy through the Fermilab QuantiSED program in the area of "Intersections of QIS and Theoretical Particle Physics." Fermilab is operated by Fermi Research Alliance, LLC under Contract No. DE-AC02-07CH11359 with the United States Department of Energy. M. C. and Y.-Y. L. would like to thank the Aspen Center for Physics, which is supported by the National Science Foundation Grant No. PHY-1607611, where part of this work has been done.

APPENDIX A: IMPORTANT INTEGRALS FOR EFFECTIVE ACTION

In the course of deriving the effective action, a number of integrals are obtained that need to be evaluated numerically. We have collated them here. Using the abbreviation

$$b^2 = \sum_{i=1}^{D-1} \sin^2 x_i, \tag{A1}$$

we have

$$I_1(\xi) = \xi\left(\frac{2}{\pi}\right)^{D-1} \int_0^{\pi/2} d^{D-1}x \frac{b}{\sqrt{\xi^2+b^2}}, \tag{A2}$$

$$I_{2a}(\xi) = \xi\left(\frac{2}{\pi}\right)^{D-1} \int_0^{\pi/2} d^{D-1}x \frac{\xi^2+2b^2}{b(\xi^2+b^2)^{3/2}}, \tag{A3}$$

$$I_{2b}(\xi) = \xi^3\left(\frac{2}{\pi}\right)^{D-1} \int_0^{\pi/2} d^{D-1}x \frac{1}{b\sqrt{\xi^2+b^2}(b+\sqrt{\xi^2+b^2})}, \tag{A4}$$

$$I_3(\xi) = \xi\left(\frac{2}{\pi}\right)^{D-1}\int_0^{\pi/2} d^{D-1}x \frac{\sin^2 x_1 \sin^2 x_2(\xi^2+2b^2)}{b^3(\xi^2+b^2)^{3/2}}, \tag{A5}$$

$$I_4(\xi) = \xi\left(\frac{2}{\pi}\right)^{D-1}\int_0^{\pi/2} d^{D-1}x \frac{\sin^2 2x_1(\xi^2+2b^2)}{b^3(\xi^2+b^2)^{-3/2}}, \tag{A6}$$

$$I_5(\xi) = \xi^2\left(\frac{2}{\pi}\right)^{D-1}\int_0^{\pi/2} d^{D-1}x \frac{1}{(\sqrt{\xi^2+b^2})(b+\sqrt{\xi^2+b^2})}, \tag{A7}$$

$$I_6(\xi) = \xi^3\left(\frac{2}{\pi}\right)^{D-1}\int_0^{\pi/2} d^{D-1}x \frac{\cos^2 x_1}{b(\xi^2+b^2)^{3/2}}, \tag{A8}$$

$$I_7(\xi) = \xi^3\left(\frac{2}{\pi}\right)^{D-1}\int_0^{\pi/2} d^{D-1}x \frac{1}{b(\xi^2+b^2)^{3/2}}. \tag{A9}$$

APPENDIX B: SERIES EXPANSION OF $I_1(\xi)$ IN TERMS OF ξ^{-2n}

For the future study of the renormalization of the Minkowski spacetime anisotropy via analytical continuation, it is useful to obtain the series expansion of the integrals Eqs. (A2)–(A9) in terms of ξ^{-1}. In this appendix, we will study $I_1(\xi)$ as an example and give the special functions related to its expansion. Expanding $(1+b^2/\xi^2)^{-1/2}$, $I_1(\xi)$ can be written as

$$\begin{aligned} I_1(\xi) &= \left(\frac{2}{\pi}\right)^{D-1}\int_0^{\pi/2} d^{D-1}x \sum_{k=0}^{\infty}\frac{\Gamma(1/2)}{\Gamma(1/2-k)k!}\frac{b^{2k+1}}{\xi^{2k}} \\ &= \sum_{k=0}^{\infty}\frac{\Gamma(1/2)}{\Gamma(1/2-k)k!\xi^{2k}}\langle b^{2k+1}\rangle_{D-1}, \end{aligned} \tag{B1}$$

where we have defined

$$\langle b^{2k+1}\rangle_{D-1} \equiv \left(\frac{2}{\pi}\right)^{D-1}\int_0^{\pi/2} d^{D-1}x\, b^{2k+1}. \tag{B2}$$

To evaluate $\langle b^{2k+1}\rangle_{D-1}$, we define the distribution function $g_{D-1}(b^2)$:

$$g_{D-1}(b^2) \equiv \left(\frac{2}{\pi}\right)^{D-1}\int_0^{\pi/2} d^{D-1}x\,\delta\left(\sum_{i=1}^{D-1}\sin^2 x_i - b^2\right) \tag{B3}$$

and thus

$$\langle b^{2k+1}\rangle_{D-1} = \int_0^{D-1} db^2 g_{D-1}(b^2) b^{2k+1}. \tag{B4}$$

The Fourier transform of g_{D-1} is

$$\begin{aligned} &\mathcal{F}\{g_{D-1}\}(\omega) \\ &= \int_0^{D-1} db^2 e^{-i\omega b^2}\left(\frac{2}{\pi}\right)^{D-1}\int_0^{\pi/2} d^{D-1}x\,\delta\left(\sum_{i=1}^{D-1}\sin^2 x_i - b^2\right) \\ &= \prod_{i=1}^{D-1}\left[\frac{2}{\pi}\int_0^{\pi/2} dx_i \exp(-i\omega\sin^2 x_i)\right] \\ &= [e^{-i\omega/2}J_0(\omega/2)]^{D-1}, \end{aligned} \tag{B5}$$

where $J_0(x)$ is the Bessel function of the first kind of order zero. The inverse Fourier transform has a simple analytic expression for $D-1 = 1, 2$:

$$g_1(b^2) = \frac{1}{\pi\sqrt{b^2(1-b^2)}}, \qquad 0 < b^2 < 1, \tag{B6}$$

$$g_2(b^2) = \frac{2}{\pi^2}K[1-(b^2-1)^2], \qquad 0 < b^2 < 2, \tag{B7}$$

where $K(k) = F(\frac{\pi}{2}|k) = \int_0^{\pi/2} d\theta(1-k\sin^2\theta)^{-1/2}$ is the incomplete elliptic integral of the first kind with the upper limit specified. For higher dimensions, we can use the following relation between g_{D-1} and g_D:

$$\begin{aligned} g_D(b^2) &= \frac{2}{\pi}\int_0^{\pi/2} dx_D g_{D-1}(b^2-\sin^2 x_D) \\ &= \int_0^1 du g_1(u) g_{D-1}(b^2-u). \end{aligned} \tag{B8}$$

For $D-1 = 1, 2, 3$, the lowest few $\langle b^{2k+1}\rangle$ are listed in Table IV. Noticing that $\langle b\rangle_{D-1}$ determines the dimensional dependence of the limit $I_1(\xi\to\infty)$, it is helpful to derive an analytical estimate of $\langle b\rangle$ in higher dimensions. As each

TABLE IV. $\langle b^{2k+1}\rangle_{D-1}$ values for $D-1 = 1, 2, 3$. Columns 2–5 are computed from the exact distribution functions Eqs. (B6), (B7), and (B8), while the last two columns are from Eqs. (B9) and (B11), respectively.

$D-1$	$\langle b\rangle_{D-1}$	$\langle b^3\rangle_{D-1}$	$\langle b^5\rangle_{D-1}$	$\langle b^7\rangle_{D-1}$	$\langle b\rangle_{\text{Gaussian}}$	$\sqrt{(D-1)/2-1/16}$
1	0.63662	0.424413	0.339531	0.291026	0.677765	0.661438
2	0.958091	1.09818	1.46262	2.13298	0.969799	0.968246
3	1.1938	1.9557	3.60865	7.22728	1.19719	1.19896

$\sin x_i^2$ has a mean value of $1/2$ and a variance of $1/8$ independently, for a large D, $g_{D-1}(b^2)$ can be approximated as the Gaussian distribution $\mathcal{N}(\frac{D-1}{2}, \frac{D-1}{8})$, with the normalization adjusted to its range $[0, D-1]$:

$$g_{D-1}(b^2) \approx \exp\left[-\frac{4(b^2-D+1)^2}{D-1}\right] \frac{2}{\sqrt{\pi(D-1)}\mathrm{Erf}(\sqrt{D-1})}, \qquad 0 < b^2 < D-1. \tag{B9}$$

Approximating the variance of b, σ_b^2 as

$$\sigma_b^2 \approx \sigma_{b^2}^2 \times \left(\frac{db}{db^2}\right)^2\Big|_{b^2=(D-1)/2} = \frac{D-1}{8} \times \left(\frac{1}{\sqrt{2(D-1)}}\right)^2 = \frac{1}{16}, \tag{B10}$$

We get

$$\langle b\rangle_{D-1} = \sqrt{\langle b^2\rangle_{D-1} - \sigma_b^2} \approx \sqrt{\frac{D-1}{2} - \frac{1}{16}}. \tag{B11}$$

Both Eqs. (B9) and (B11) give good approximation for $\langle b\rangle_{D-1}$ for $D-1 = 2, 3$, as listed in Table IV. Using Eq. (B11), the large anisotropy limit in higher dimensions reads,

$$I_1(\xi \to \infty) = \langle b\rangle_{D-1} \approx \sqrt{\frac{D-1}{2} - \frac{1}{16}}. \tag{B12}$$

[1] R. P. Feynman, Simulating physics with computers, Int. J. Theor. Phys. **21**, 467 (1982).
[2] S. Lloyd, Universal quantum simulators, Science **273**, 1073 (1996).
[3] S. P. Jordan, H. Krovi, K. S. Lee, and J. Preskill, BQP-completeness of scattering in scalar quantum field theory, Quantum **2**, 44 (2018).
[4] C. W. Bauer *et al.*, Quantum simulation for high energy physics, arXiv:2204.03381.
[5] I. Raychowdhury and J. R. Stryker, Loop, string, and hadron dynamics in SU(2) Hamiltonian lattice gauge theories, Phys. Rev. D **101**, 114502 (2020).
[6] A. Alexandru, P. F. Bedaque, S. Harmalkar, H. Lamm, S. Lawrence, and N. C. Warrington (NuQS Collaboration), Gluon field digitization for quantum computers, Phys. Rev. D **100**, 114501 (2019).
[7] Z. Davoudi, I. Raychowdhury, and A. Shaw, Search for efficient formulations for Hamiltonian simulation of non-Abelian Lattice Gauge Theories, Phys. Rev. D **104**, 074505 (2021).
[8] A. Ciavarella, N. Klco, and M. J. Savage, A trailhead for quantum simulation of SU(3) Yang-Mills lattice gauge theory in the local multiplet basis, Phys. Rev. D **103**, 094501 (2021).
[9] A. Kan and Y. Nam, Lattice quantum chromodynamics and electrodynamics on a universal quantum computer, arXiv:2107.12769.
[10] A. Alexandru, P. F. Bedaque, R. Brett, and H. Lamm, The spectrum of qubitized QCD: Glueballs in a $S(1080)$ gauge theory, Phys. Rev. D **105**, 114508 (2022).
[11] I. Raychowdhury and J. R. Stryker, Solving Gauss's law on digital quantum computers with loop-string-hadron digitization, Phys. Rev. Res. **2**, 033039 (2020).
[12] E. Zohar, J. I. Cirac, and B. Reznik, Cold-Atom Quantum Simulator for SU(2) Yang-Mills Lattice Gauge Theory, Phys. Rev. Lett. **110**, 125304 (2013).
[13] E. Zohar, J. I. Cirac, and B. Reznik, Quantum simulations of gauge theories with ultracold atoms: Local gauge invariance from angular momentum conservation, Phys. Rev. A **88**, 023617 (2013).
[14] E. Zohar and M. Burrello, Formulation of lattice gauge theories for quantum simulations, Phys. Rev. D **91**, 054506 (2015).
[15] E. Zohar, A. Farace, B. Reznik, and J. I. Cirac, Digital lattice gauge theories, Phys. Rev. A **95**, 023604 (2017).
[16] J. Bender, E. Zohar, A. Farace, and J. I. Cirac, Digital quantum simulation of lattice gauge theories in three spatial dimensions, New J. Phys. **20**, 093001 (2018).
[17] J. F. Haase, L. Dellantonio, A. Celi, D. Paulson, A. Kan, K. Jansen, and C. A. Muschik, A resource efficient approach for quantum and classical simulations of gauge theories in particle physics, Quantum **5**, 393 (2021).

[18] C. W. Bauer and D. M. Grabowska, Efficient representation for simulating U(1) gauge theories on digital quantum computers at all values of the coupling, arXiv:2111.08015.
[19] Y. Ji, H. Lamm, and S. Zhu (NuQS Collaboration), Gluon field digitization via group space decimation for quantum computers, Phys. Rev. D **102**, 114513 (2020).
[20] A. Bazavov, S. Catterall, R. G. Jha, and J. Unmuth-Yockey, Tensor renormalization group study of the non-abelian higgs model in two dimensions, Phys. Rev. D **99**, 114507 (2019).
[21] A. Bazavov, Y. Meurice, S.-W. Tsai, J. Unmuth-Yockey, and J. Zhang, Gauge-invariant implementation of the Abelian Higgs model on optical lattices, Phys. Rev. D **92**, 076003 (2015).
[22] J. Zhang, J. Unmuth-Yockey, J. Zeiher, A. Bazavov, S. W. Tsai, and Y. Meurice, Quantum Simulation of the Universal Features of the Polyakov Loop, Phys. Rev. Lett. **121**, 223201 (2018).
[23] J. Unmuth-Yockey, J. Zhang, A. Bazavov, Y. Meurice, and S.-W. Tsai, Universal features of the Abelian Polyakov loop in $1+1$ dimensions, Phys. Rev. D **98**, 094511 (2018).
[24] J. F. Unmuth-Yockey, Gauge-invariant rotor Hamiltonian from dual variables of 3D $U(1)$ gauge theory, Phys. Rev. D **99**, 074502 (2019).
[25] U.-J. Wiese, Towards quantum simulating QCD, Nucl. Phys. **A931**, 246 (2014).
[26] D. Luo, J. Shen, M. Highman, B. K. Clark, B. DeMarco, A. X. El-Khadra, and B. Gadway, A framework for simulating gauge theories with dipolar spin systems, Phys. Rev. A **102**, 032617 (2020).
[27] R. C. Brower, D. Berenstein, and H. Kawai, Lattice gauge theory for a quantum computer, *Proc. Sci.* LATTICE2019 (2019) 112 [arXiv:2002.10028].
[28] S. V. Mathis, G. Mazzola, and I. Tavernelli, Toward scalable simulations of lattice gauge theories on quantum computers, Phys. Rev. D **102**, 094501 (2020).
[29] H. Liu and S. Chandrasekharan, Qubit regularization and qubit embedding algebras, Symmetry **14**, 305 (2022).
[30] E. Gustafson, Prospects for simulating a qudit based model of $(1+1)$d scalar QED, Phys. Rev. D **103**, 114505 (2021).
[31] E. Gustafson, Noise improvements in quantum simulations of sQED using qutrits, arXiv:2201.04546.
[32] Scaling IonQ's quantum computers: The roadmap (2020), https://ionq.com/posts/december-09-2020-scaling-quantum-computer-roadmap.
[33] IBM's roadmap for building an open quantum software ecosystem (2021), https://research.ibm.com/blog/quantum-development-roadmap.
[34] H. Neven, Day 1 opening keynote by Hartmut Neven (quantum summer symposium 2020) (2020), https://www.youtube.com/watch?v=TJ6vBNEQReU.
[35] B. Şahinoğlu and R. D. Somma, Hamiltonian simulation in the low energy subspace, NPJ Quantum Inf. **7**, 119 (2021).
[36] T. Hatomura, State-dependent error bound for digital quantum simulation of driven systems, Phys. Rev. A **105**, L050601 (2022).
[37] S. P. Jordan, K. S. M. Lee, and J. Preskill, Quantum algorithms for quantum field theories, Science **336**, 1130 (2012).
[38] E. Campbell, Random Compiler for Fast Hamiltonian Simulation, Phys. Rev. Lett. **123**, 070503 (2019).
[39] C. Cirstoiu, Z. Holmes, J. Iosue, L. Cincio, P. J. Coles, and A. Sornborger, Variational fast forwarding for quantum simulation beyond the coherence time, npj Quantum Inf. **6**, 82 (2020).
[40] J. Gibbs, K. Gili, Z. Holmes, B. Commeau, A. Arrasmith, L. Cincio, P. J. Coles, and A. Sornborger, Long-time simulations with high fidelity on quantum hardware, arXiv:2102.04313.
[41] Y.-X. Yao, N. Gomes, F. Zhang, T. Iadecola, C.-Z. Wang, K.-M. Ho, and P. P. Orth, Adaptive variational quantum dynamics simulations, PRX Quantum **2**, 030307 (2021).
[42] D. W. Berry, A. M. Childs, R. Cleve, R. Kothari, and R. D. Somma, Simulating Hamiltonian Dynamics with a Truncated Taylor Series, Phys. Rev. Lett. **114**, 090502 (2015).
[43] G. H. Low and I. L. Chuang, Hamiltonian simulation by qubitization, Quantum **3**, 163 (2019).
[44] A. Rajput, A. Roggero, and N. Wiebe, Quantum error correction with gauge symmetries, arXiv:2112.05186.
[45] N. Klco and M. J. Savage, Hierarchical qubit maps and hierarchically implemented quantum error correction, Phys. Rev. A **104**, 062425 (2021).
[46] K. Stannigel, P. Hauke, D. Marcos, M. Hafezi, S. Diehl, M. Dalmonte, and P. Zoller, Constrained Dynamics via the Zeno Effect in Quantum Simulation: Implementing non-Abelian Lattice Gauge Theories with Cold Atoms, Phys. Rev. Lett. **112**, 120406 (2014).
[47] J. R. Stryker, Oracles for Gauss's law on digital quantum computers, Phys. Rev. A **99**, 042301 (2019).
[48] J. C. Halimeh and P. Hauke, Reliability of Lattice Gauge Theories, Phys. Rev. Lett. **125**, 030503 (2020).
[49] H. Lamm, S. Lawrence, and Y. Yamauchi (NuQS Collaboration), Suppressing coherent gauge drift in quantum simulations, arXiv:2005.12688.
[50] M. C. Tran, Y. Su, D. Carney, and J. M. Taylor, Faster digital quantum simulation by symmetry protection, PRX Quantum **2**, 010323 (2021).
[51] J. C. Halimeh, H. Lang, J. Mildenberger, Z. Jiang, and P. Hauke, Gauge-symmetry protection using single-body terms, PRX Quantum **2**, 040311 (2021).
[52] J. C. Halimeh and P. Hauke, Staircase prethermalization and constrained dynamics in lattice gauge theories, arXiv:2004.07248.
[53] J. C. Halimeh, V. Kasper, and P. Hauke, Fate of lattice gauge theories under decoherence, arXiv:2009.07848.
[54] J. C. Halimeh, R. Ott, I. P. McCulloch, B. Yang, and P. Hauke, Robustness of gauge-invariant dynamics against defects in ultracold-atom gauge theories, Phys. Rev. Res. **2**, 033361 (2020).
[55] M. Van Damme, J. C. Halimeh, and P. Hauke, Gauge-symmetry violation quantum phase transition in lattice gauge theories, arXiv:2010.07338.
[56] V. Kasper, T. V. Zache, F. Jendrzejewski, M. Lewenstein, and E. Zohar, Non-Abelian gauge invariance from dynamical decoupling, arXiv:2012.08620.

[57] J. C. Halimeh, H. Lang, and P. Hauke, Gauge protection in non-Abelian lattice gauge theories, New J. Phys. **24**, 033015 (2022).
[58] X.-Q. Luo, S.-H. Guo, H. Kroger, and D. Schutte, Improved lattice gauge field Hamiltonian, Phys. Rev. D **59**, 034503 (1999).
[59] J. Carlsson and B. H. McKellar, Direct improvement of Hamiltonian lattice gauge theory, Phys. Rev. D **64**, 094503 (2001).
[60] M. Carena, H. Lamm, Y.-Y. Li, and W. Liu, Improved Hamiltonians for Quantum Simulations, Phys. Rev. Lett. **129**, 051601 (2022).
[61] H. Lamm and S. Lawrence, Simulation of Nonequilibrium Dynamics on a Quantum Computer, Phys. Rev. Lett. **121**, 170501 (2018).
[62] S. Harmalkar, H. Lamm, and S. Lawrence (NuQS Collaboration), Quantum simulation of field theories without state preparation, arXiv:2001.11490.
[63] E. J. Gustafson and H. Lamm, Toward quantum simulations of $\mathbb{Z}_2$ gauge theory without state preparation, Phys. Rev. D **103**, 054507 (2021).
[64] Y. Yang, B.-N. Lu, and Y. Li, Accelerated quantum Monte Carlo with mitigated error on noisy quantum computer, PRX Quantum **2**, 040361 (2021).
[65] D. C. Hackett, K. Howe, C. Hughes, W. Jay, E. T. Neil, and J. N. Simone, Digitizing gauge fields: Lattice Monte Carlo results for future quantum computers, Phys. Rev. A **99**, 062341 (2019).
[66] Y. Ji, H. Lamm, and S. Zhu, Gluon digitization via character expansion for quantum computers, arXiv:2203.02330.
[67] T. Hartung, T. Jakobs, K. Jansen, J. Ostmeyer, and C. Urbach, Digitising SU(2) gauge fields and the freezing transition, Eur. Phys. J. C **82**, 237 (2022).
[68] K. Osterwalder and R. Schrader, Axioms for euclidean Green's functions, Commun. Math. Phys. **31**, 83 (1973).
[69] K. Osterwalder and R. Schrader, Axioms for euclidean Green's functions. 2., Commun. Math. Phys. **42**, 281 (1975).
[70] M. Carena, H. Lamm, Y.-Y. Li, and W. Liu, Lattice renormalization of quantum simulations, Phys. Rev. D **104**, 094519 (2021).
[71] G. Clemente, A. Crippa, and K. Jansen, Strategies for the determination of the running coupling of $(2+1)$-dimensional QED with quantum computing, arXiv:2206.12454.
[72] C. J. Hamer, M. D. Sheppeard, W.-h. Zheng, and D. Schutte, Universality for SU(2) Yang-Mills theory in $(2+1)$-dimensions, Phys. Rev. D **54**, 2395 (1996).
[73] T. M. R. Byrnes, M. Loan, C. J. Hamer, F. D. R. Bonnet, D. B. Leinweber, A. G. Williams, and J. M. Zanotti, The Hamiltonian limit of $(3+1)$-D SU(3) lattice gauge theory on anisotropic lattices, Phys. Rev. D **69**, 074509 (2004).
[74] A. N. Ciavarella and I. A. Chernyshev, Preparation of the SU(3) lattice Yang-Mills vacuum with variational quantum methods, Phys. Rev. D **105**, 074504 (2022).
[75] R. C. Farrell, I. A. Chernyshev, S. J. M. Powell, N. A. Zemlevskiy, M. Illa, and M. J. Savage, Preparations for quantum simulations of quantum chromodynamics in $1+1$ dimensions: (I) Axial gauge, arXiv:2207.01731.
[76] S. A. Rahman, R. Lewis, E. Mendicelli, and S. Powell, Self-mitigating Trotter circuits for SU(2) lattice gauge theory on a quantum computer, Phys. Rev. D **106**, 074502 (2022).
[77] B. S. DeWitt, Quantum theory of gravity. 2. The manifestly covariant theory, Phys. Rev. **162**, 1195 (1967).
[78] B. S. DeWitt, Quantum theory of gravity. 3. Applications of the covariant theory, Phys. Rev. **162**, 1239 (1967).
[79] J. Honerkamp, The Question of invariant renormalizability of the massless Yang-Mills theory in a manifest covariant approach, Nucl. Phys. **B48**, 269 (1972).
[80] G. 't Hooft, An algorithm for the poles at dimension four in the dimensional regularization procedure, Nucl. Phys. **B62**, 444 (1973).
[81] C. G. Callan, Jr., R. F. Dashen, and D. J. Gross, A theory of hadronic structure, Phys. Rev. D **19**, 1826 (1979).
[82] A. Hasenfratz and P. Hasenfratz, The connection between the lambda parameters of lattice and continuum QCD, Phys. Lett. **93B**, 165 (1980).
[83] R. F. Dashen and D. J. Gross, The relationship between lattice and continuum definitions of the gauge theory coupling, Phys. Rev. D **23**, 2340 (1981).
[84] A. Gonzalez-Arroyo and C. Korthals Altes, Asymptotic freedom scales for any single plaquette action, Nucl. Phys. **B205**, 46 (1982).
[85] M. Giordano, Renormalization of gauge theories on general anisotropic lattices and high-energy scattering in QCD, Phys. Rev. D **92**, 034514 (2015).
[86] A. Hasenfratz and P. Hasenfratz, The scales of Euclidean and Hamiltonian lattice QCD, Nucl. Phys. **B193**, 210 (1981).
[87] F. Karsch, SU(N) gauge theory couplings on asymmetric lattices, Nucl. Phys. **B205**, 285 (1982).
[88] C. Hamer, Scales of Euclidean and Hamiltonian lattice gauge theory in three-dimensions, Phys. Rev. D **53**, 7316 (1996).
[89] Y. Iwasaki and S. Sakai, The Λ parameter for improved lattice gauge actions, Nucl. Phys. **B248**, 441 (1984).
[90] M. Garcia Perez and P. van Baal, One loop anisotropy for improved actions, Phys. Lett. B **392**, 163 (1997).
[91] S. Sakai, T. Saito, and A. Nakamura, Anisotropic lattice with improved gauge actions. 1. Study of fundamental parameters in weak coupling regions, Nucl. Phys. **B584**, 528 (2000).
[92] S. Sakai and A. Nakamura, Improved gauge action on an anisotropic lattice. 2. Anisotropy parameter in the medium coupling region, Phys. Rev. D **69**, 114504 (2004).
[93] I. T. Drummond, A. Hart, R. R. Horgan, and L. C. Storoni, One loop calculation of the renormalized anisotropy for improved anisotropic gluon actions on a lattice, Phys. Rev. D **66**, 094509 (2002).
[94] S. Capitani, Lattice perturbation theory, Phys. Rep. **382**, 113 (2003).
[95] G. Cella, U. M. Heller, V. K. Mitrjushkin, and A. Vicere, The Coulomb law in the pure gauge U(1) theory on a lattice, Phys. Rev. D **56**, 3896 (1997).
[96] M. Loan, T. Byrnes, and C. Hamer, Hamiltonian study of improved u(1) lattice gauge theory in three dimensions, Phys. Rev. D **70**, 014504 (2004).
[97] M. J. Teper, SU(N) gauge theories in $(2+1)$-dimensions, Phys. Rev. D **59**, 014512 (1998).

[98] D. Petcher and D. H. Weingarten, Monte Carlo calculations and a model of the phase structure for gauge theories on discrete subgroups of SU(2), Phys. Rev. D **22**, 2465 (1980).
[99] M. Creutz, L. Jacobs, and C. Rebbi, Experiments with a Gauge Invariant Ising System, Phys. Rev. Lett. **42**, 1390 (1979).
[100] M. Creutz, L. Jacobs, and C. Rebbi, Monte Carlo study of abelian lattice gauge theories, Phys. Rev. D **20**, 1915 (1979).
[101] M. Hasenbusch and K. Pinn, Surface tension, surface stiffness, and surface width of the three-dimensional Ising model on a cubic lattice, Physica (Amsterdam) **192A**, 342 (1993).
[102] M. Caselle, R. Fiore, F. Gliozzi, M. Hasenbusch, K. Pinn, and S. Vinti, Rough interfaces beyond the Gaussian approximation, Nucl. Phys. **B432**, 590 (1994).
[103] V. Agostini, G. Carlino, M. Caselle, and M. Hasenbusch, The spectrum of the $(2+1)$-dimensional gauge Ising model, Nucl. Phys. **B484**, 331 (1997).
[104] M. S. Alam, S. Hadfield, H. Lamm, and A. C. Y. Li (SQMS Collaboration), Primitive quantum gates for dihedral gauge theories, Phys. Rev. D **105**, 114501 (2022).
[105] T. R. Klassen, The anisotropic Wilson gauge action, Nucl. Phys. **B533**, 557 (1998).